Indonesian Physical Review
Volume 08 Issue 01, January 2025
P-ISSN: 2615-1278, E-ISSN: 2614-7904

Design and Build a Microcontroller Based Dip Coater Tool with an Automatic Calibration System

Nizar Rizki Rahman[1*], Imam Sya'roni[2], Anton Hartanto [3], Agus Dwi Prasetyono[4], Irfan Subiantoro[4]
[1] *Physics Education, Universitas Negeri Surabaya, Indonesia*
[2] *Graduate of Automation and Control, National Taiwan University of Science and Technology, Taiwan*
[3] *Mechanical Engineering, Universitas Negeri Surabaya, Indonesia*
[4] *Physics, Universitas Negeri Surabaya, Indonesia*

Corresponding Authors E-mail: nizarrahman@unesa.ac.id

Article Info

Article info:
Received: 12-07-2024
Revised: 29-10-2024
Accepted: 11-11-2024

Keywords:
Microcontroller; Dip-coater; thin films; calibration

How To Cite:
N. R. Rahman, I. Sya'roni, A. Hartanto, A. D. Prasetyono, and I. Subiantoro, "Design and build a microcontroller based on dip-coater tool with an automatic calibration system", Indonesian Physical Review, vol. 8, no. 1, p 48-61, 2025.

DOI:
https://doi.org/10.29303/ipr.v8i1.364

Abstract

Dip-coating is essential for coating materials evenly, as imperfections like macropores can impact material properties. This project presents a digitally controlled dip-coating tool that manages withdrawal speed, immersion time, and speed via a microcontroller with an automatic calibration system. Employing a stepper motor and mathematical formula approach, the tool achieves high precision by automatically adjusting dipping parameters, with key metrics including resolution-dependent V_l, calibration speed V_{pc} and calibration targets $t_{pc,}$ and S_c. The system reaches stable calibration at $V_{ms} = V_{pc}$. ensuring rapid, accurate calibration and minimizing errors to 0-2% across 20 to 650 steps. Additionally, the tool's energy-efficient design consumes less power than other dip-coating systems, providing both durability and accuracy.

Introduction

Technology is a primary driver of research advancements [1]. The latest innovations play a crucial role in ensuring research outputs aligned with theoretical expectations and initial analyses. Technological progress has rapidly evolved from conventional to automated systems [2], especially in microstructure applications, such as thin films. These thin layers, made from materials like organic, inorganic, metallic, or non-metallic compounds, exhibit properties ranging from conductors and semiconductors to superconductors and insulators [3]. In

materials engineering, especially for thin films, commonly used materials include In_2O_3, SnO_2, TiO_2, ZnO, and ITO. Significant research has been conducted on various thin film fabrication processes, highlighting their importance in this field.

Several methods are used to manufacture thin films, including sol-gel dip coating [4], spray pyrolysis [5], RF magnetron sputtering [6], and sol-gel spin coating [7]. Among these, sol-gel dip coating is particularly popular due to its ease of use and ability to produce high-quality, uniform layers. This method allows for precise layer-by-layer application, facilitating sequential coating or further characterization processes [8]. Dip-coating is a coating method that involves immersing the material in a solution for a specific time and then removing the material from the dipping place. Dip-coating is a coating method that effectively adds strength to each coated material and is accurate [9][10]Dip-coating is an effective method to reduce the impact of macropores by creating layers that are sufficiently solid to support subsequent coatings. This technique produces a sequence of layers that seamlessly blend over controlled distances [11]. Several parameters are essential for controlling the quality of layers in dip-coating. These parameters include immersion speed, soaking time, and material withdrawal speed from the coating material. A single parameter error can greatly impact the quality of the coated layer. For example, the drawing speed is critical in dip-coating, as it directly influences layer thickness. Variations in speed yield different thicknesses, while factors such as material viscosity and solid content also affect the coating's uniformity [11][12]. Therefore, achieving precise alignment between input and processed values is essential for consistent results. Previous research [13] developed a dip-coating system for thin-layer formation; however, its transmission relied on a three-gear mechanism for vertical movement, which suffered from efficiency losses due to friction, sliding effects, and the inherent inefficiencies of each gear type.

Previous research [14] developed a dip-coating system using a servo motor, but without a calibration equation or control system, resulting in high linear speed errors. Similarly, other studies [15][16] created low-cost dip coaters with manual speed control, lacking digital precision. To address these limitations, this research aims to develop a microcontroller-based dip coater that digitally controls dipping speed, soak time, and withdrawal speed through an automatic calibration system using a mathematical approach. Microcontroller-based systems offer key advantages, including low cost, easy maintenance, digital recording, and customizable programming for user-defined settings [12][17][18]. The innovation in this study lies in combining a mathematical calibration approach with a microcontroller system, providing precise step accuracy. Additionally, the tool's automatic calibration system employs a point-capture method, enabling real-time measurement data storage and self-calibration in response to detected errors.

Theory and Calculation

Dip Coater

A dip coater is a tool used to make a thin layer by dipping the media into the coating material. In general, this tool should have immersion, soaking, drawing, and evaporation features. Dyeing is the first process in the dip coater tool feature. At a constant speed, the medium is dipped into the coating solution. Based on the type of substrate, a pre-treatment process will usually be carried out before this step. The second feature is immersion. That is, the media remains in the solution for a specified time, after which a withdrawal process is carried out. In this case, the media is pulled out of the solution. As the media is pulled out, a thin film

layer begins to deposit. The thickness of the layer directly depends on the speed of the substrate withdrawal. The slower the pull, the thinner the coating layer produced. Then the last feature is evaporation. Namely, the media will be dried in air at room temperature. The quality of the coating produced in this way, however, is inconsistent, and therefore, this approach is not appropriate for industrial processes [19][20]. Dip coating has been widely used for research purposes due to its straightforward approach.

Dip-Coating Method

The dip coating method is also known as a method of making a thin layer by dipping the media and coating material. Similar to screen printing, this method uses coating materials that contain insoluble liquids and solids in the fabrication process. The coating material is a combination of ceramic powder, solvent, binder and dispersing agent. The process of making a thin layer using the dip coating method is that first, the media will drop into the coating material solution at a certain speed. After that, the media is left in the coating material solution for a specific time, and the next stage is that the media will be pulled at a certain speed, and the coating material will stick to it. The media will then be dried in air at room temperature [21]. The smoothness and thickness of the coating can be controlled by changing the content of solids in the coating material and the speed of pulling the material from the coating material solution. Layers with a thickness of several microns to hundreds of microns can be produced using this method [22]. The usual duration for immersing the media in the coating agent solution is about 30 seconds [23]. Figure 1 below illustrates the dip coating method.

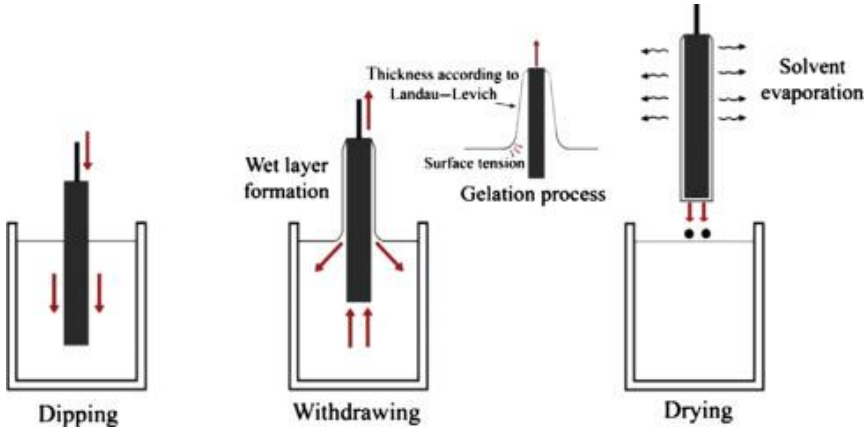

Figure 1. Material coating using dip coating method [24].

Point Capture Calibration

The calibration method for this tool is to use a point capture calibration system, which captures calibration data based on several speed points to increase the accuracy and precision of the tool and minimize errors to be more accurate. Several calibrated speed points will be looked for that are close to the speed that will be run and then compared with the speed that will be run. After that, the speed to be run will be adjusted to the speed error point during calibration.

$$V_{ms} = \frac{V_l \times V_{pc} \times t_{pc}}{s_c} \quad (1)$$

Equation (1)[25] above will be used as the stepper motor speed equation according to the calibration data on the dip coater tool that will be made. In accordance with the equation above, to get the stepper motor speed V_{ms} (step/s), four variables are needed, namely, V_l,

which is the linear speed to be set (mm/s), V_{pc}, which is the calibration speed at the speed point (step/s), t_{pc} which is the calibration time at point speed (s), and s_c which is the calibration distance (mm).

To find out the maximum linear speed of the tool, we can change equation (1) to the equation (2) [25] below.

$$V_l = \frac{V_{ms} \times s_c}{V_{pc} \times t_{pc}} \quad (2)$$

Since at maximum speed $V_{ms} = V_{pc}$, then

$$Max\ V_l = \frac{s_c}{t_{pc}} \quad (3)$$

Experimental Method

This research uses the Research and Development method [26][27]. The research flow diagram is made according to the steps in the types of research and development. The research flow diagram can be shown in Figure 2.

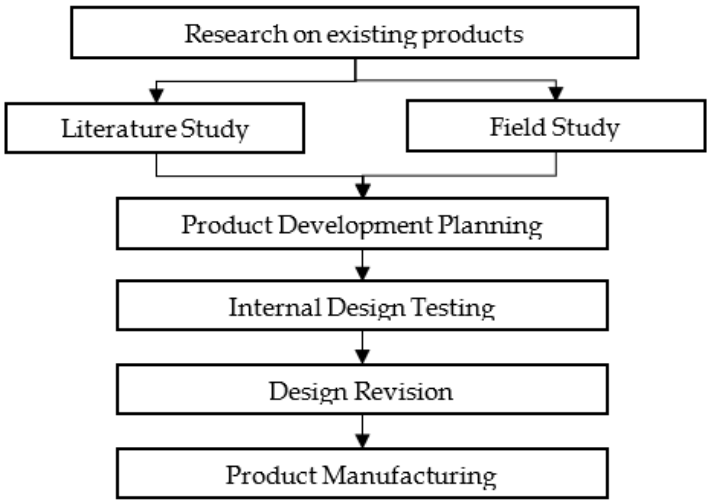

Figure 2. Research method

The first stage of research and development involves identifying the issues associated with the research object, in this case, the dip coater tool. Problem identification is accomplished through a comprehensive study of existing products, enabling the researcher to understand the challenges and design a solution accordingly. The subsequent phase consists of a literature and field study to gather the necessary data for product development. This data collection is conducted through a literature review, involving books, journals, and other resources on the research topic, as well as field studies through direct observation and analysis of tool components. Once the relevant data is acquired, the tool's design is developed using appropriate software, such as 3D design applications, PCB Wizard, and Arduino IDE (with an Arduino Nano selected for its compact size and functionality). The design is then tested internally using software simulations and individual part evaluations. If issues are identified during testing, the design is revised accordingly. After internal testing and revisions, the final step involves product manufacturing, followed by data testing, focusing on electrical performance and tool calibration data as specified by the research objectives..

The microcontroller-based dip coater system comprises key components, including an LCD, control buttons, a stepper motor, an Arduino microcontroller, a rotary screw, and a power supply. In this setup, the stepper motor drives the rotary screw, enabling precise upward and downward movement of the coating arm. The microcontroller modulates the stepper motor's rotation speed, thus controlling the dipping arm's rate during immersion and withdrawal from the coating liquid. This configuration allows for precise manipulation of coating parameters, which is essential for achieving consistent layer quality in thin film applications.

Results and Discussion

3D Design and Real Tool

The results of the 3D design of the tool are shown in the Figure 3 below.

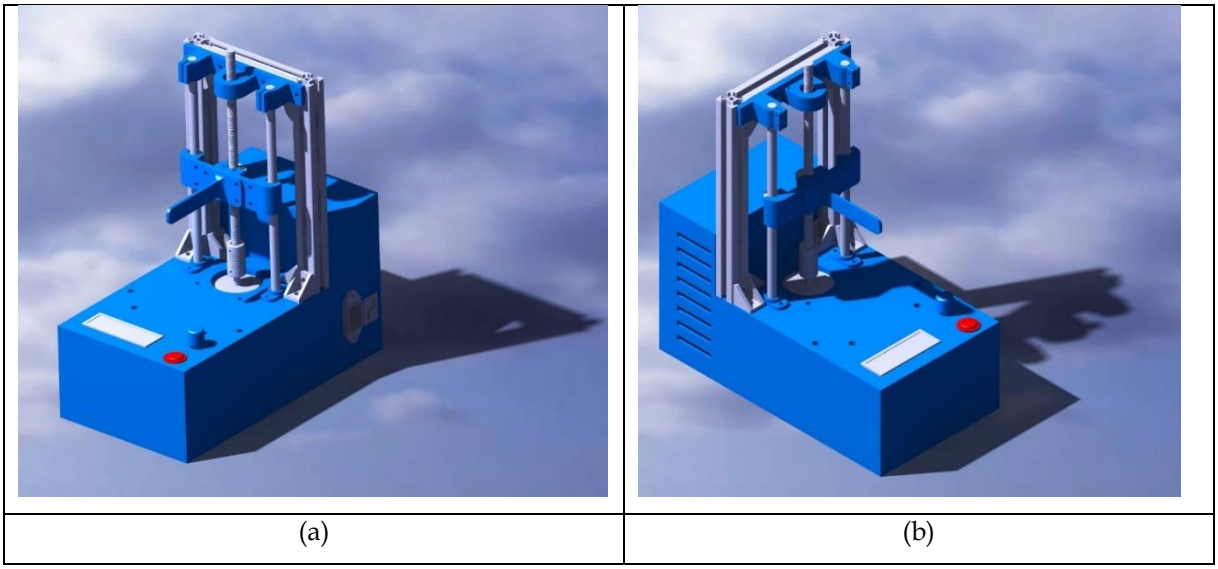

(a) (b)

Figure 3. 3D Design of The Tool (a) Right Side of View (b) Left Side of View

Meanwhile, Figure 4 shows the results of making the tool. The design dimensions of the tool are 140 mm long, 261 mm wide, and 288 mm high, with the main working space being 70 mm long, 90 mm wide and 150 mm high. The design of this tool has three parts. The first part is the electrical part, which contains the LCD electrical components, encoder, reset button, and electrical components inside the tool. The second part is the main workspace, which is in the middle of the other parts. The main workspace contains a Nema 23 stepper motor with a resolution of 200 steps/r (motor) and 25 steps/mm (linear movement), a lead screw that has a pitch of 2 mm, and other moving components. The third part is the power supply section, which contains the power supply for the tool's component resources. From equation 1, we must choose value of V_l for system. V_l is linear velocity. So, it must convert to step. The resolution from stepper is 25 steps/mm. So, for the first step as 20 step/mm. We use determination between resolution and V_{pc} to get V_l for system. More large data on Table 1. After getting V_l because these parameters can be changed, we can use equation 1 to get V_{ms} with different V_l in from different parameters resulting in V_{pc}, t_{pc} in the same one value S_c.

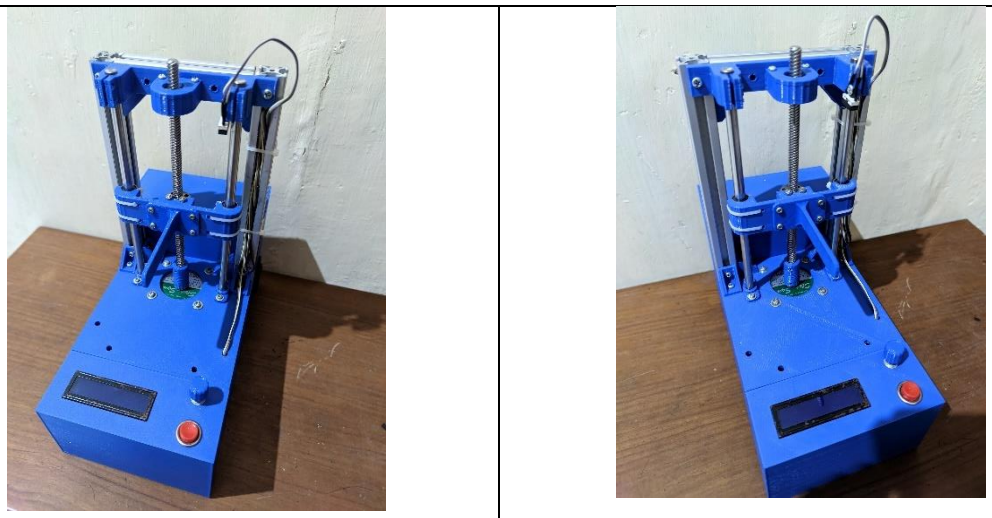

(a) (b)

Figure 4. Result of The Tool (a) Right Side of View (b) Left Side of View

Electrical Component

The electrical circuit of the dip coater tool that is made can be seen in the picture below.

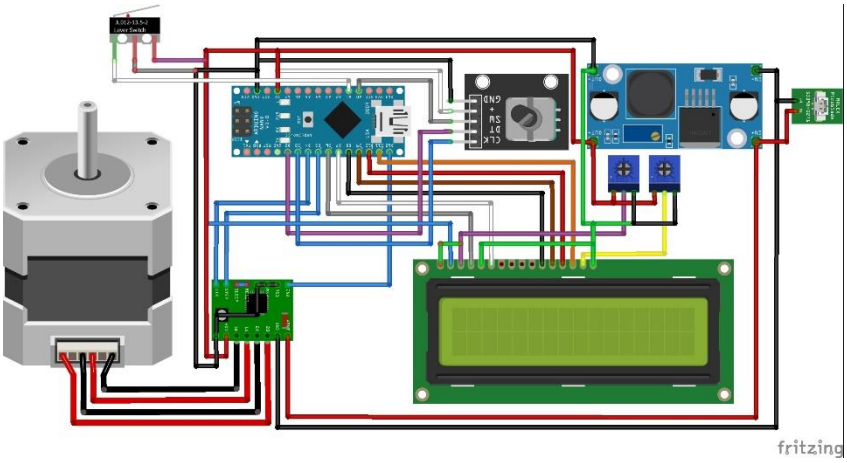

Figure 5. Electrical Schematic

Flowchart Diagram of Tool Program

The tool program process flow diagram shows how the program process runs on the tool. There are three main programs in this tool, namely the calibration section, the variable setting section, and the program section that runs the tool drive. The image below is a flow diagram of the tool program process.

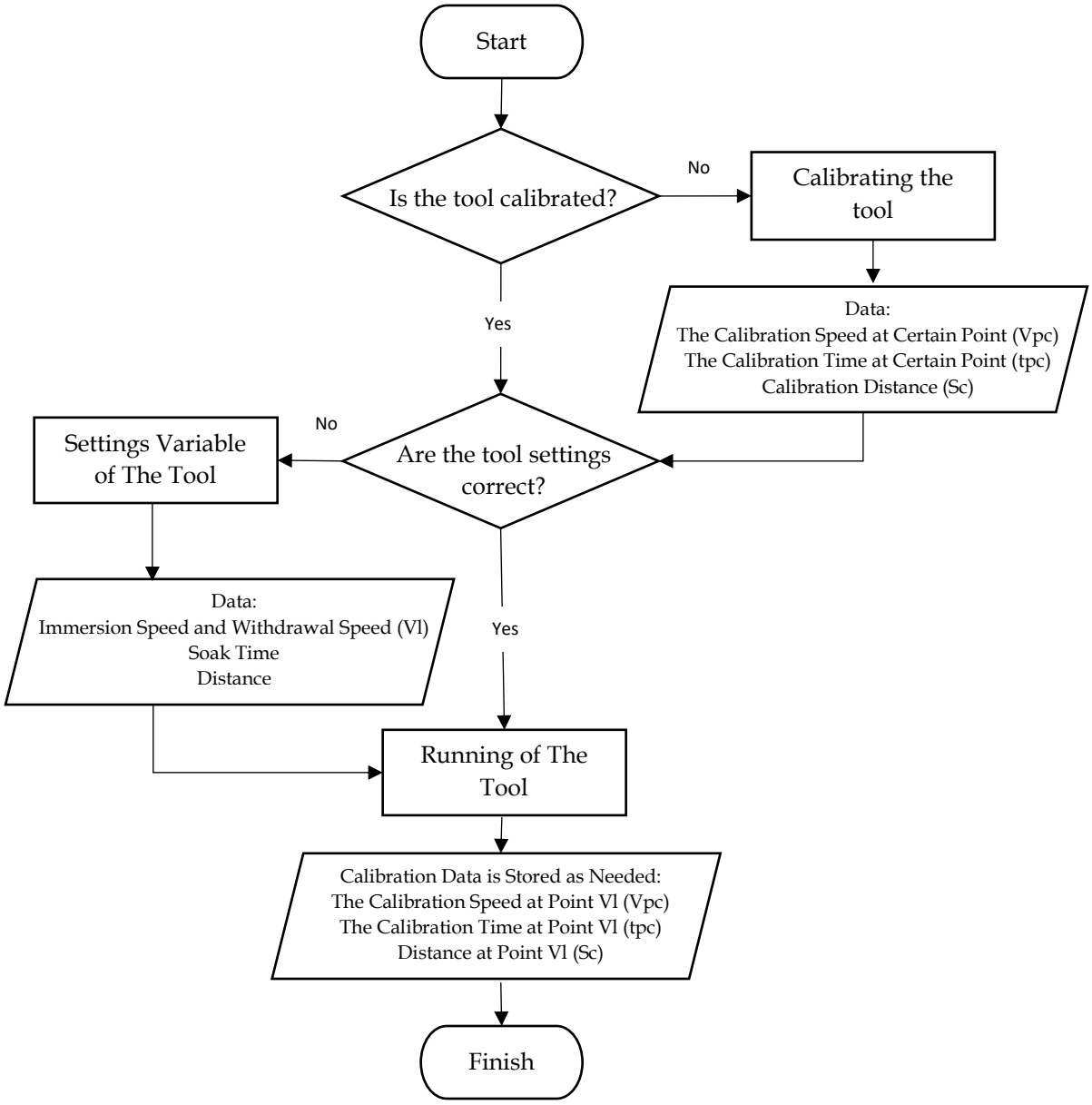

Figure 6. Flowchart Diagram of Tool Program

This study adopts a research and development methodology to design and test the dip coating instrument. The research flow is depicted in Figure 6, illustrating the stages of the instrument's development. The initial stage involves calibration of the dip coating prototype, which, before calibration, requires adjustments to several critical parameters, including Vpc, tpc, and Sc. Once the prototype is calibrated, an automated calibration method is applied. This method involves capturing calibration points at each stage, allowing for the determination of errors associated with the parameters. After the automatic calibration process is executed, the final parameter values are established based on the tool's operation, particularly those affecting immersion depth, immersion duration, and immersion speed.

Calibration Data

Calibration data testing uses a calibration distance (s_c) of 20 mm, 40 mm, 60 mm, and 80 mm. The following variable data will be used according to the formulated equation.

Manipulated variables : V_l (mm/s), s_c (mm)
Control variables : V_{pc} (step/s), V_{pc} $linear$ (mm/s), t_{pc}(ms), R_s (step/mm)
Response variable : V_{ms} (step/s)

The following is a table of tool calibration results at calibration distances of 20 mm, 40 mm, 60 mm and 80 mm.

Table 1. Tool calibration data at calibration distances of 20 mm, 40 mm, 60 mm and 80 mm.

s_c = 20 mm				s_c = 40 mm			
V_{ms} (step/s)	V_l (mm/s)	V_{pc} (step/s)	t_{pc} (ms)	V_{ms} (step/s)	V_l (mm/s)	V_{pc} (step/s)	t_{pc} (ms)
20	0.80	20	25007	**20**	0.80	20	50013
50	2.00	50	10008	**50**	2.00	50	20016
100	4.00	100	5015	**100**	4.00	100	10032
151	6.00	150	3348	**151**	6.00	150	6694
201	8.00	200	2516	**201**	8.00	200	5030
252	10.00	250	2015	**252**	10.00	250	4032
302	12.00	300	1678	**302**	12.00	300	3354
353	14.00	350	1442	**353**	14.00	350	2883
405	16.00	400	1266	**405**	16.00	400	2531
456	18.00	450	1126	**456**	18.00	450	2252
507	20.00	500	1014	**507**	20.00	500	2028
558	22.00	550	923	**559**	22.00	550	1847
609	24.00	600	846	**609**	24.00	600	1691
659	26.00	650	780	**660**	26.00	650	1562

s_c = 60 mm				s_c = 80 mm			
V_{ms} (step/s)	V_l (mm/s)	V_{pc} (step/s)	t_{pc} (ms)	V_{ms} (step/s)	V_l (mm/s)	V_{pc} (step/s)	t_{pc} (ms)
20	0.80	20	75021	**20**	0.80	20	100027
50	2.00	50	30025	**50**	2.00	50	40034
100	4.00	100	15045	**100**	4.00	100	20061
151	6.00	150	10041	**151**	6.00	150	13389
201	8.00	200	7546	**201**	8.00	200	10060
252	10.00	250	6048	**252**	10.00	250	8064
302	12.00	300	5032	**302**	12.00	300	6710
353	14.00	350	4326	**353**	14.00	350	5768
405	16.00	400	3796	**405**	16.00	400	5063
456	18.00	450	3379	**456**	18.00	450	4504
507	20.00	500	3041	**507**	20.00	500	4056
559	22.00	550	2771	**559**	22.00	550	3693
609	24.00	600	2538	**609**	24.00	600	3382
660	26.00	650	2342	**660**	26.00	650	3123

The calibration results presented in Table 1 demonstrate that the use of V_1 from resolution impacts the outcome of the V_{ms} in the system. In an ideal system, the values of V_{pc} and V_{ms} should be identical at every target within the same distance. The next step involves calculating the error of the automated calibration system in the dip coating tool using the root mean square error (RMSE). The real value obtained from V_{pc} is compared to the speed value of V_{ms} derived from the system, with one observation taken for each data collection. The error value is computed using the Root Mean Square Error (RMSE) formula [28], as shown in Equation 4.

$$RMSE = \sqrt{\sum_{i=1}^{n} \frac{(\hat{y}_i - y_i)^2}{n}} \quad (4)$$

Table 2. Error Percentage V_{ms} for V_{pc} with Root Mean Square Error

V_{pc} (step/s)	Percentage of error V_{ms} against V_{pc}			
	s_c = 20 mm	s_c = 40 mm	s_c = 60 mm	s_c = 80 mm
20	0%	0%	0%	0%
50	0%	0%	0%	0%
100	0%	0%	0%	0%
150	0%	0%	0%	0%
200	1%	1%	1%	1%
250	1%	1%	1%	1%
300	1%	1%	1%	1%
350	1%	1%	1%	1%
400	1%	1%	1%	1%
450	1%	1%	1%	1%
500	1%	1%	1%	1%
550	2%	2%	2%	2%
600	1%	1%	1%	1%
650	1%	2%	1%	1%

Based on the results presented in Table 2, the calibration distance does not significantly affect the percentage of error produced. The error percentage, as described in the table, represents the deviation of the actual speed from the calibration reference speed. The error percentage falls within the range of 0% to 2%, indicating that the stepper motor speed is inherently stable and accurate. The primary factor influencing the calibration time is the response time of the microcontroller and other electrical components in the network. This error can be minimized to nearly 0% using the point capture calibration equation. Once the tool is used, the linear speed data is stored in the tool's database, allowing the system to automatically calibrate the tool to match or closely approximate the previously recorded speed. If the speed database does not exist, the tool can still function based on the available data. In comparison to previous research [13][15], the use of a stepper motor for controlling the arm movement in this dip coater enhances the accuracy of the arm's motion compared to a servo motor. The stepper motor operates based on voltage pulses, with each movement precisely calculated in degrees. Additionally, the calibration equation further refines the movement speed, minimizing errors. The dip coater's settings can be controlled directly via the encoder and LCD on the tool, allowing for easy adjustment without the need for a computer connection.

Electrical Data

In this electrical data section, the electrical power requirements are described when the tool is in standby mode, the tool is working at minimum speed, and the tool is working at maximum speed. This is important because power requirements can also affect several other tools in the laboratory.

The following is an electrical table for the dip coater tool that has been made.

Table 3. Dip Coater Electrical Data

Velocity (mm/s)	Voltage (Volt)	Current (Ampere)	Power (Watt)	Information
0.00	220	0.121	26.62	Idle/Standby
0.04	220	0.126	27.72	Running
0.80	220	0.129	28.38	Running
2.00	220	0.131	28.82	Running
4.00	220	0.134	29.48	Running
6.00	220	0.136	29.92	Running
8.00	220	0.142	31.24	Running
10.00	220	0.153	33.66	Running
12.00	220	0.158	34.76	Running
14.00	220	0.167	36.74	Running
16.00	220	0.173	38.06	Running
18.00	220	0.182	40.04	Running
20.00	220	0.190	41.80	Running
22.00	220	0.201	44.22	Running
24.00	220	0.216	47.52	Running
26.00	220	0.221	48.62	Running

The graph below shows the relationship between speed and the electrical power needed by the tool to work.

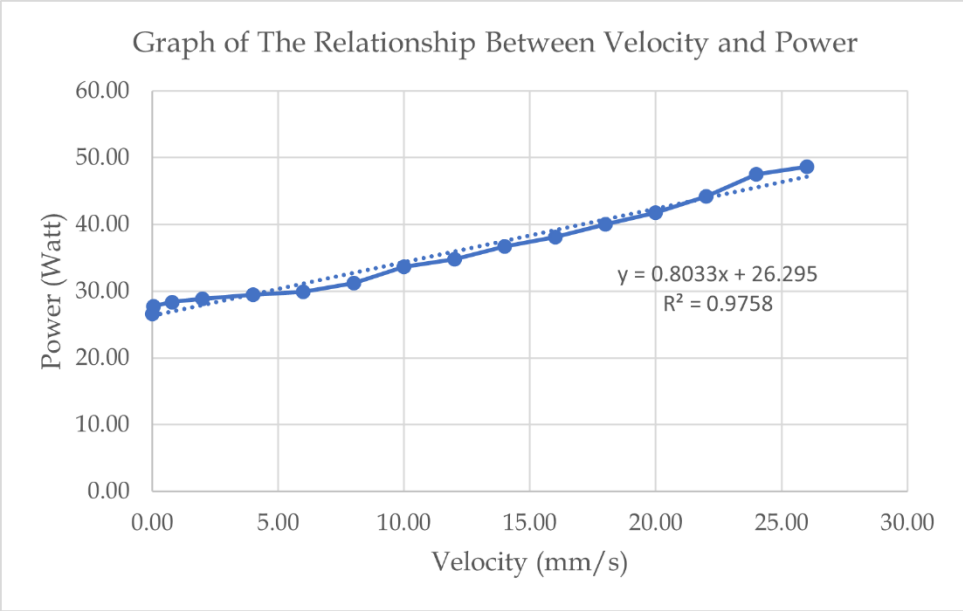

Figure 7. Graph of The Relationship Between Velocity and Power

Based on table 3, the electrical specifications of the tool when the tool is not running is 26.62 Watts. Meanwhile, when running, the tool requires a minimum of 27.72 Watts of power and a maximum of 48.62 Watts. Based on the graph that has been presented, the relationship between tool speed and the energy used is directly proportional to the linearity level of 97.58%. Compared with previous research [14], the power used is relatively low because this tool uses a stepper motor without any additional gears, which makes the motor movement more efficient.

Conclusion

The constructed tool has dimensions of 140 mm in length, 261 mm in width, and 288 mm in height, with the main working area measuring 70 mm in length, 90 mm in width, and a maximum height of 150 mm. It consists of three main components: the electrical system, the main work area, and the power supply. The tool operates with three primary programs: the calibration section, the variable setting section, and the program that controls the tool's drive.

According to the calibration data presented, the calibration distance does not significantly affect the error percentage produced. The error percentage calculated using the Root Mean Square Error (RMSE), ranges from 0% (for calibration distances of 20, 50, 100, and 150) to 1% (for distances of 200, 250, 300, 350, 400, 450, 500, 600, and 650), and reaches 2% at 550. The average error is 0.78571%, which can be minimized to nearly 0% by utilizing the point capture calibration equation.

Regarding the electrical specifications, the tool consumes 26.62 Watts when idle. During operation, the tool requires a minimum of 27.72 Watts and a maximum of 48.62 Watts. Based on the presented graph, there is a direct proportionality between the tool's speed and the energy consumption.

Acknowledgment

This research was supported by the Universitas Negeri Surabaya (UNESA) under its LPPM competitive functional education staff research scheme.

References

[1] A. C. Adamuthe and G. T. Thampi, "Technology forecasting: A case study of computational technologies," Technol Forecast Soc Change, vol. 143, pp. 181–189, 2019, doi: https://doi.org/10.1016/j.techfore.2019.03.002.

[2] Y. Wang, X. Wu, Y. Wang, and X. Zhou, "Fuzzy logic-based feedback control system for the frequency stabilization of external-cavity semiconductor lasers," Int J Optomechatronics, vol. 14, no. 1, pp. 44–52, 2020, doi: 10.1080/15599612.2020.1828516.

[3] T. Naito, "Modern history of organic conductors: An overview," Crystals (Basel), vol. 11, no. 7, Jul. 2021, doi: 10.3390/cryst11070838.

[4] T. Chen, W. Fan, P. Xu, X. Chen, M. Qiu, and Y. Fan, "Construction of asymmetric ceramic membranes with identical source interlayer on fly ash support by dip-coating," J Eur Ceram Soc, vol. 44, no. 15, Dec. 2024, doi: 10.1016/j.jeurceramsoc.2024.116765.

[5] H. Xu, D. Cheng, L. Zhao, H. Dong, and B. Liu, "Numerical study of bischofite precursor droplet evaporation and thermal decomposition for spray pyrolysis systems," Chem Eng Sci, vol. 301, Jan. 2025, doi: 10.1016/j.ces.2024.120680.

[6] D. Chaussende et al., "Investigation of amorphous-SiC thin film deposition by RF magnetron sputtering for optical applications," Mater Sci Semicond Process, vol. 182, Nov. 2024, doi: 10.1016/j.mssp.2024.108673.

[7] E. El Mahboub et al., "Investigation of kesterite to stannite phase transition and band gap engineering in Cu2Zn1-xCoxSnS4 thin films prepared by sol-gel spin coating," Appl Surf Sci, vol. 672, Nov. 2024, doi: 10.1016/j.apsusc.2024.160848.

[8] T. Chen, W. Fan, P. Xu, X. Chen, M. Qiu, and Y. Fan, "Construction of asymmetric ceramic membranes with identical source interlayer on fly ash support by dip-coating," J Eur Ceram Soc, vol. 44, no. 15, Dec. 2024, doi: 10.1016/j.jeurceramsoc.2024.116765.

[9] P. Zhang et al., "Mass-Produced Flexible Strain Sensors Based on Dip-Coating and Water Bath for Human–Computer Interaction," IEEE Sens J, vol. 23, no. 2, pp. 1497–1506, 2023, doi: 10.1109/JSEN.2022.3225104.

[10] Y. Zhao, N. Song, X. Xu, and F. Gao, "Research on the Fabrication of Ultrasensitive Fabry–Pérot Pressure Sensor Based on Dip-Coating Method," IEEE Sens J, vol. 23, no. 14, pp. 15614–15621, 2023, doi: 10.1109/JSEN.2023.3281778.

[11] J. Li et al., "Robust, breathable and antibacterial superamphiphobic cotton fabrics prepared by layer-by-layer dip coating," Appl Surf Sci, vol. 669, Oct. 2024, doi: 10.1016/j.apsusc.2024.160582.

[12] K. Aggoun, L. Chaal, J. Creus, R. Sabot, B. Saidani, and M. Jeannin, "Marine corrosion resistance of CeO2/Mg (OH)2 mixed coating on a low alloyed steel," Surf Coat Technol, vol. 372, pp. 410–421, Aug. 2019, doi: 10.1016/j.surfcoat.2019.05.053.

[13] V. H. Guerrero, L. J. Segura, and D. Loza, "Mechanical and Electronic Systems of an Open Source Based Spin and Dip Coater." [Online]. Available: https://www.researchgate.net/publication/299560607

[14] A. Mukhsinin and M. Ficky Afrianto, "RANCANG BANGUN ALAT PEMBUAT LAPISAN TIPIS METODE DIP COATING BERBASIS ARDUINO UNO," Jurnal Ilmu Fisika dan Pembelajarannya), vol. 3, no. 2, pp. 76–83, 2019.

[15] C. Dunlap et al., "Design and fabrication of a low-cost and programmable dip coating machine Specifications table," Hardware X, 2022, doi: 10.17605/OSF.IO/3AB6Z.

[16] C. Dunlap, "Design and Fabrication of A Low-Cost and Programmable Dip Coating Machine [Online]," OSF. Accessed: Jul. 23, 2024. [Online]. Available: https://osf.io/twcb5

[17] N. Fauza et al., "Microcontroller-Based Mechanics Experiments in Physics Learning: Systematic Literature Review Using PRISMA," Jurnal Penelitian Pendidikan IPA, vol. 9, no. 9, pp. 558–568, Sep. 2023, doi: 10.29303/jppipa. v9i9.5258.

[18] E. Syahruddin Kaseng, A. Syifani, A. Muhammad, and A. Mukhlis, "Development and Working Test of Microcontroller-based Automatic Seedling Tools for Hydroponic Systems," vol. 14, no. 2, 2024.

[19] L. W. McKeen, Permeability Properties of Plastics and Elastomers: Fourth Edition. 2016.

[20] S. Bose, "Chapter 6 - Oxidation- and Corrosion-Resistant Coatings," in High Temperature Coatings (Second Edition), S. Bose, Ed., Butterworth-Heinemann, 2018, pp. 97–198. doi: https://doi.org/10.1016/B978-0-12-804622-7.00006-1.

[21] I. A. Neacşu, A. I. Nicoară, O. R. Vasile, and B. Ş. Vasile, "Chapter 9 - Inorganic micro- and nanostructured implants for tissue engineering," in Nanobiomaterials in Hard Tissue Engineering, A. M. Grumezescu, Ed., William Andrew Publishing, 2016, pp. 271–295. doi: https://doi.org/10.1016/B978-0-323-42862-0.00009-2.

[22] L. Wu et al., "Dip-Coating Process Engineering and Performance Optimization for Three-State Electrochromic Devices," Nanoscale Res Lett, vol. 12, 2017, doi: 10.1186/s11671-017-2163-0.

[23] A. Permadi, S. Yuliani, I. Wahyuningsih, and I. Satar, "Optimization of thin layers of coated turmeric extract (Curcuma longa L) tablets using a dipping method," Media Farmasi: Jurnal Ilmu Farmasi, vol. 19, no. 1, p. 1, Mar. 2022, doi: 10.12928/mf.v19i1.20130.

[24] T. Choudhary and Sanjay, "Computational analysis of IR-SOFC: Thermodynamic, electrochemical process and flow configuration dependency," Int J Hydrogen Energy, vol. 41, no. 2, pp. 1259–1271, 2016, doi: https://doi.org/10.1016/j.ijhydene.2015.10.098.

[25] A. Hartanto, N. R. Rahman, I. Sya'roni, A. D. Prasetyono, and I. Subiantoro, "Automatic Calibration Equation for Microcontroller Based Dip Coater Tools with Point Capture Calibration System [Manuscript submitted for publication]," Surabaya, 2024.

[26] I. Sya'roni, A. Hartanto, N. R. Rahman, and I. Subiantoro, "Indonesian Physical Review Microcontroller Base Spin Coating Design and IoT Data Monitoring and Storage," 2023, doi: 10.29303/ip.

[27] S. Jabeen, S. K. Srinivasan, S. Shuja, and M. A. L. Dubasi, "A Formal Verification Methodology for FPGA-Based Stepper Motor Control," IEEE Embed Syst Lett, vol. 7, no. 3, pp. 85–88, 2015, doi: 10.1109/LES.2015.2450677.

[28] M. Ćalasan, I. Radonjić, M. Micev, M. Petronijević, and L. Pantić, "Voltage root mean square error calculation for solar cell parameter estimation: A novel g-function approach," Heliyon, vol. 10, no. 18, Sep. 2024, doi: 10.1016/j.heliyon. 2024.e37887.